

****Volume Title****

*ASP Conference Series, Vol. **Volume Number***

****Author****

© ****Copyright Year**** *Astronomical Society of the Pacific*

Vortices in the solar photosphere

S. Shelyag¹, V. Fedun², R. Erdélyi², F.P. Keenan¹, and M. Mathioudakis¹

¹*Astrophysics Research Centre, Department of Mathematics and Physics, Queen's University, Belfast, BT7 1NN, UK*

²*Solar Physics and Space Plasma Research Centre (SP²RC), Department of Applied Mathematics, University of Sheffield, Sheffield, S3 7RH, UK*

Abstract. Using numerical simulations of the magnetised solar photosphere and radiative diagnostics of the simulated photospheric models, we further analyse the physical nature of magnetic photospheric intergranular vortices. We confirm the magnetic nature of the vortices and find that most MHD Umov-Poynting flux is produced by horizontal vortex motions in the magnetised intergranular lanes. In addition, we consider possible ways to directly observe photospheric magnetic vortices using spectropolarimetry. Although horizontal plasma motions cannot be detected in the spectropolarimetric observations of solar disk centre, we find an observational signature of photospheric vortices in simulated observations of Stokes-*V* amplitude asymmetry close to the solar limb. Potential ways to find the vortices in the observations are discussed.

1. Introduction

The recent discovery of vortex motions in the solar photosphere has raised the question of the role of photospheric vortices in the energy transport from the solar interior to the outer atmosphere. Bonet et al. (2008) showed that Magnetic Bright Points (MBPs) are subject to vortex motions in the intergranular lanes. An analysis of small-scale intergranular vortex structures and their motions has been presented by Vargas Domínguez et al. (2011). High-resolution multi-wavelength observations (Wedemeyer-Böhm & Rouppe van der Voort 2009) suggest that the vortices, corresponding to MBP motions, coincide spatially with chromospheric swirls. Moll et al. (2011) reported on the formation of small-scale intergranular vortices in weak magnetic field simulations of the solar photosphere. Shelyag et al. (2011a,b) have demonstrated that solar atmospheric vorticity generation, which reveals itself as both MBP rotary motions and upper-atmospheric swirls, efficiently occurs only in intergranular magnetic field concentrations, and the vorticity generation in the upper solar photosphere is essentially a magnetic phenomenon. Vortex motions in small-scale magnetic field concentrations can generate a variety of magneto-hydrodynamic waves (Erdélyi & Fedun 2007; Jess et al. 2009; Fedun et al. 2011b), which propagate to the outer layers of solar atmosphere, where the energy can be dissipated (see e.g. Zaqarashvili et al. 2011). This mechanism may be responsible for the transport of energy from the solar interior towards the higher layers of the solar atmosphere, including the corona.

This paper is devoted to some further analysis of photospheric magnetic vortices. We demonstrate the generation of positive, directed outwards Umov-Poynting flux and

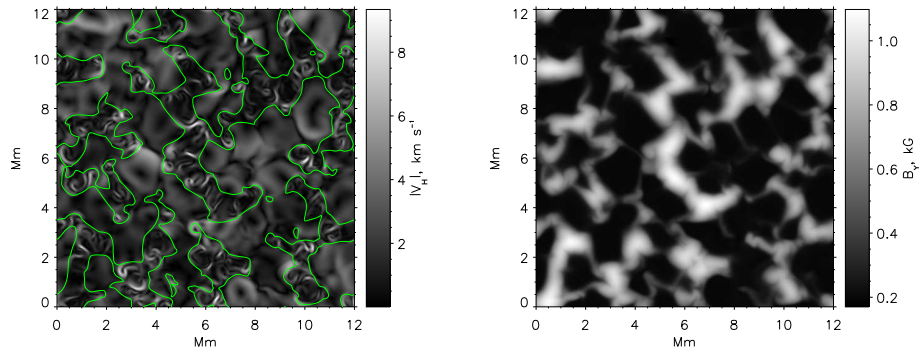


Figure 1. Horizontal slices of the modulus of the horizontal components of velocity (left panel) and vertical component of magnetic field (right panel) measured at the height $y = 500$ km above the average continuum formation level in the simulation domain. Regions with the vertical magnetic field strength larger than 400 G, bounded by contours on the left panel, are covered by small-scale vortex structures, visually different from granular outflows.

also show that the vertical component of the Umov-Poynting flux vector is generated mainly by horizontal vortex motions. This finding is confirmed by the numerical simulation of an individual cylindrically symmetric magnetic flux tube embedded in a quiet convectively stable atmospheric model. We also perform detailed spectropolarimetric diagnostics with the FeI 630.2 nm line to explore possibilities for observing intergranular vortex motions close to the solar limb.

The structure of this paper is organised as follows. In Section 2, we briefly describe our simulation setup and show the mechanisms to produce magnetic photospheric vorticity. We demonstrate the presence of Umov-Poynting flux connected to photospheric vortices in Section 3, and further support this evidence by performing a test flux tube simulation in Section 4, and discuss possibilities for observing photospheric vorticity in Section 5. Our conclusions are given in Section 6.

2. Vorticity generation is the solar photosphere

We use the MURaM code (Vögler et al. 2005) to undertake simulations of the magnetised photosphere. The code is extensively used in the solar physics community and is described in great detail in the literature (see e.g. Shelyag et al. 2004; Rempel et al. 2009). Our simulation procedure is similar to that described in Shelyag et al. (2011a), and here we provide only a brief description. The numerical domain is $12 \times 12 \times 1.4$ Mm³ size, resolved by $480 \times 480 \times 100$ grid cells. A uniform magnetic field of 200 G strength is introduced into a well-developed, non-magnetic photospheric convection snapshot, and a sequence of snapshots, containing the photospheric plasma parameters, is recorded. Here we use a well-developed snapshot of photospheric magnetoconvection recorded after 1 hour of the physical simulation time, during which the magnetic field has collapsed into the intergranular lanes and the simulation has achieved statistical stability.

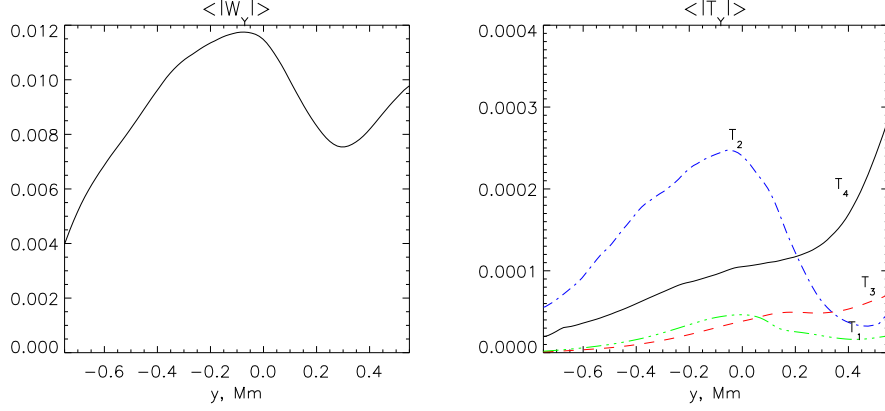


Figure 2. Dependence of the horizontally-averaged modulus of the vertical component of vorticity (left panel) and dependences of the T_1 (dash-dot-dotted line), T_2 (dash-dotted line), T_3 (dashed line) and T_4 (solid line) terms of vorticity equation (Eq. 1, right panel) on height in the simulation domain. Zero height represents the approximate level of the photosphere.

In Figure 1, the horizontal slices of the modulus of horizontal components of velocity $v_h = (v_x^2 + v_z^2)^{1/2}$ and the vertical component of the magnetic field B_y are shown in the left and right panels, respectively (note that in our notation x and z are the horizontal directions, while y is the vertical). The contours on the left panel bound the regions with $B_y > 400\text{G}$, corresponding to the magnetised intergranular lanes. It is evident from the figure that the intergranular vortex motions, visible as small-scale semi-circular structures in the left panel of the plot, are bounded by the magnetic field contours, and, thus are clearly co-located with and abundantly cover the strong intergranular magnetic field regions. Also, there is clearly a difference in the geometry of the intergranular magnetic vortex flows and granular outflows. The granular flows have dark granular centres, corresponding to the upflows with small horizontal velocities, surrounded by stronger horizontal outflows, which do not show any small-scale structure.

We analyse the small-scale vortex features in the magnetised intergranular lanes, using the vorticity equation, derived from the equations of magneto-hydrodynamics (MHD). The process of vorticity production was demonstrated by Shelyag et al. (2011a). Here we provide only a brief description. The MHD vorticity equation can be derived by taking the curl of the MHD momentum equation, separating the magnetic and non-magnetic terms and decomposing the magnetic term into two:

$$\rho \frac{D}{Dt} \frac{\boldsymbol{\omega}}{\rho} = \overbrace{(\boldsymbol{\omega} \cdot \nabla) \mathbf{v}}^{T_1} - \overbrace{\nabla \frac{1}{\rho} \times \nabla p_g}^{T_2} - \overbrace{\nabla \frac{1}{\rho} \times [\nabla p_m - (\mathbf{B} \cdot \nabla) \mathbf{B}]}^{T_3} + \overbrace{\frac{1}{\rho} \nabla \times [(\mathbf{B} \cdot \nabla) \mathbf{B}]}^{T_4}. \quad (1)$$

Here, T_1 is the vortex tilting term, T_2 the baroclinic vorticity generation term, T_3 the magnetic baroclinic term, and T_4 the magnetic field tension term. As shown by Shelyag et al. (2011a), the latter term T_4 is mainly responsible for vorticity production in the upper photosphere, while T_2 generates vorticity deeper in the photosphere and in the convection zone. This is further demonstrated by the right panel of Figure 2, where the height dependences of the terms are plotted on the same scale. The figure

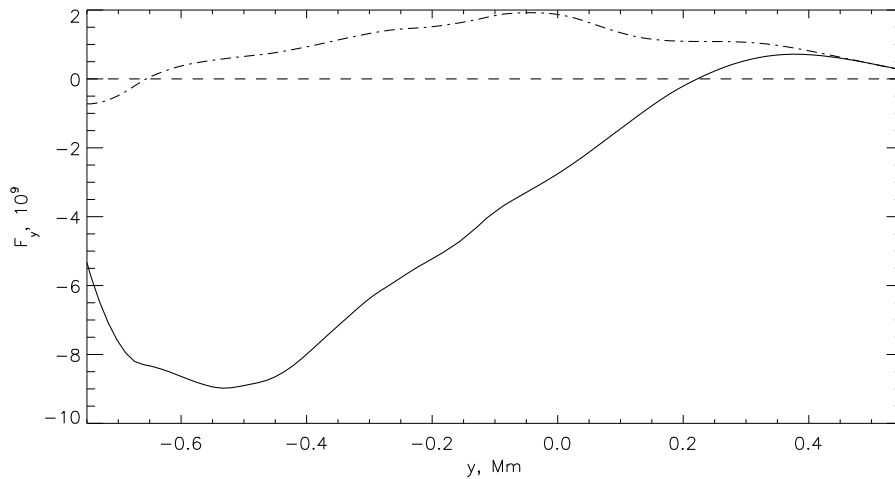


Figure 3. Horizontally-averaged dependences of the vertical component of Umov-Poynting flux vector (solid line) and the vertical component of the Umov-Poynting flux vector, generated by horizontal plasma motions (dash-dotted line), on depth.

shows that T_4 (solid line) becomes greater than T_2 (dash-dotted line) at heights 0.2 Mm above the approximate continuum formation level, while T_2 is about twice as large at the level of continuum formation $y = 0$. The terms T_1 and T_3 do not play a significant role in the vorticity production. It also should be noted that T_2 and T_4 act in an opposite way and suppress each other, as it is evident from the opposite signs of these terms in Equation 1. In the left panel of Figure 2, the dependence of the horizontally averaged modulus of the vertical component of vorticity is shown. It can be seen from the figure that, in accordance to the physical mechanism outlined above, the vorticity takes its local minimum at $y = 0.2$ Mm, takes its maximum, caused by the baroclinic term T_2 at $y = 0$ and increases towards the upper photosphere in the region $y > 0.2$ Mm.

3. Umov-Poynting flux in the photospheric magnetic vortices

The plasma motions in magnetic fields can generate Umov-Poynting flux. In magneto-hydrodynamics, the Umov-Poynting flux vector \mathbf{F} is defined as

$$\mathbf{F} = \mathbf{B} \times (\mathbf{v} \times \mathbf{B}), \quad (2)$$

where \mathbf{v} is the plasma velocity field, and \mathbf{B} is the magnetic field. It is of interest to measure the vertical, (y) component of the Umov-Poynting flux vector (F_y), connected to the magnetic vortex motions in the solar photosphere, since it can be responsible for the energy transport from the solar interior to the outer solar atmosphere. Figure 3 shows the dependence of the horizontally-averaged vertical component of the Umov-Poynting flux vector on height in the simulated model. As the plot demonstrates, F_y is negative in the convection zone and in the low photosphere, while it becomes positive (directed outwards) in the upper part of the photosphere above $y > 0.2$ Mm, in the same range where the magnetic tension term is greater than the baroclinic hydrodynamic

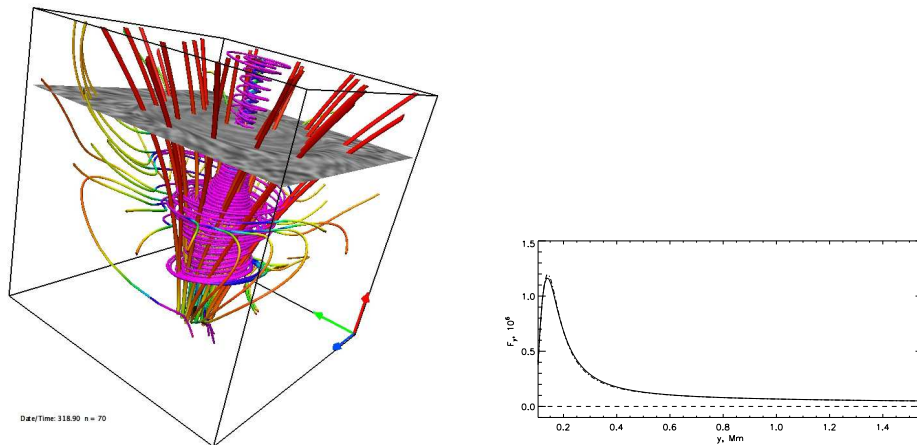


Figure 4. Simulation of individual flux tube. Left image - magnetic field lines (red), velocity field lines (red-blue-green-violet) and total velocity at 1 Mm height (greyscale) in the domain. Right image - vertical component of Umov-Poynting flux.

term, $T_4 > T_2$ (see Section 2). In our simulation we find the behaviour of the vertical component of the Umov-Poynting flux vector to be similar to the result demonstrated by Steiner et al. (2008). However, it should be noted that Steiner et al. (2008) use a much weaker magnetic field in their simulation, and demonstrate a different mechanism of the Umov-Poynting flux generation.

To confirm the connection between the photospheric magnetic vortices and the Umov-Poynting flux, we analyse the effect of horizontal motions on the vertical component of the Umov-Poynting flux by setting artificially the vertical component of velocity v_y to zero in Equation 2. The depth dependence of $F_{y,v_y=0}$ computed for $v_y = 0$ is shown in Figure 3 as the dash-dotted line. As can be seen, $F_{y,v_y=0}$ is generally positive, except from a small part of the domain deep in the convection zone, and $F_{y,v_y=0}$ is nearly equal to the full vertical component of the Umov-Poynting flux in the region $y > 0.4$ Mm. It is, therefore, clear that the positive vertical component of the Umov-Poynting flux in the upper photosphere is generated by horizontal vortex motions in the photospheric magnetic field concentrations.

4. Vortex motions in individual magnetic flux tube embedded into a convectively stable solar atmospheric model

To further establish a relation between photospheric vortex motions in the intergranular magnetic field concentrations and Umov-Poynting flux, we performed a test simulation of a cylindrically-symmetric magnetic flux tube embedded into a convectively stable model of the solar atmosphere, using the Sheffield Advanced Code (Shelyag et al. 2008). In this simulation, the computational domain has a physical size of 1.2 Mm^3 resolved by $100 \times 100 \times 196$ grid points in the x , z and y directions respectively, with a lower boundary located at the photospheric level $y = 0$, and magnetic field configuration as described in detail by Fedun et al. (2011a,c). The expanding flux tube with the magnetic field strength of $B = 1.2 \text{ kG}$ at the footpoint (height $y = 0.0 \text{ Mm}$) is in magneto-hydrostatic equilibrium with the non-magnetic ambient plasma outside.

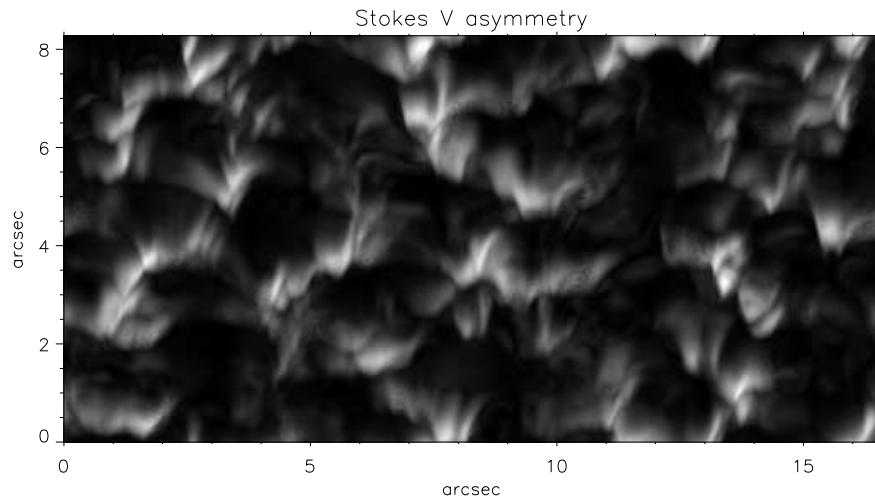


Figure 5. Simulated Stokes- V amplitude asymmetry of the FeI 630.2 nm absorption line at 60° angular distance to the north from the solar disk centre.

We perturb the initially stable configuration with a velocity source located at height $y = 0.1$ Mm in the photosphere and acting for the first 200 seconds of the simulation. The interaction of the source with the model creates a vortex with the horizontal velocity amplitude $v_h \approx 1 \text{ km s}^{-1}$ at the footpoint of the magnetic flux tube (see Figure 4; this image was created with VAPOR 3D visualisation package (Clyne et al. 2007)). This vortex also generates the vertical Umov-Poynting flux, directed outwards to the upper solar atmosphere. The flux F_y is shown in the right panel of Figure 4. Similarly to our previous analysis in Section 3, we compare the total vertical component of the Umov-Poynting flux with that generated by horizontal motions in the magnetic vortex. The two curves representing these are plotted as solid and dash-dotted lines, respectively. Since these are virtually indistinguishable, we conclude that the vertical component of Umov-Poynting flux is generated by horizontal vortex motions. It should be noted that only a qualitative comparison of this result with the Umov-Poynting flux amplitudes, provided in Section 3, is possible due to the different nature of these simulations.

5. Radiative diagnostics of the photospheric magnetic vortices

Intergranular vortices, being horizontal motions in the solar photosphere, are not easy to observe. The fast changing nature and small size of vortex structures, requires high spatial and temporal resolution. Such observations have been used to track spiral motions of photospheric features, including MBPs in the intergranular lanes (Bonet et al. 2008). However, it is not possible to directly observe the velocity field of vortices in the upper photosphere using MBP tracking as the photospheric MBPs are localised intensity enhancements which are formed deep in the photosphere and do not fully cover the intergranular lanes.

Therefore, we consider the possibility of directly observing photospheric magnetic vortex signatures using spectropolarimetry. Horizontal motions do not reveal them-

selves in spectropolarimetry at disk centre. However, the situation is different near the solar limb as the horizontal motions show a strong component along the line-of-sight. Also, due to the magnetic nature of the photospheric vorticity, the asymmetry of Stokes- V profiles (see e.g. Shelyag et al. 2007, and the references therein), featuring in the regions with gradients of line-of-sight magnetic field and velocity due to layered structure of photospheric vortices (Shelyag et al. 2011b), is expected. We analyse this possibility by performing radiative transport diagnostics in the photospheric model, inclined by 60° to the north from the solar disk centre, with the FeI 630.2 nm photospheric absorption line. The synthetic Stokes- V amplitude asymmetry image, shown in Figure 5, demonstrates strong signal in the intergranular lanes, as expected. Also, the Stokes- V asymmetry features in the image have shapes closely resembling the cylinder-like, layered vortex structures, demonstrated by Shelyag et al. (2011b). One of the clearest features of this type is located at (3, 4) arcseconds in the image. The spatial resolution required to resolve this feature is estimated to be about 0.1 arcsec in low light conditions due to limb darkening. Thus, future instruments for high-resolution spectropolarimetric solar observations with large apertures, such as the planned ATST, may be able to resolve these features in detail.

6. Conclusions

Using direct numerical modelling of solar photospheric plasma, we simulate the vortex motions in the magnetised intergranular lanes. Through two different approaches of simulations of magneto-convection, and direct modelling of the magnetic flux tube embedded into the solar atmosphere, we demonstrate that magnetised intergranular lanes generate significant amount of Umov-Poynting flux, directed outwards to the higher layers of the solar atmosphere, and show that the main part of this flux is produced by horizontal vortex motions. Finally, we demonstrate the possibility to directly observe photospheric vortices using high-resolution spectropolarimetric observations close to the solar limb.

Acknowledgments. This work has been supported by the UK Science and Technology Facilities Council (STFC). R. Erdélyi acknowledges M. Kéray for patient encouragement and is grateful to NSF, Hungary (OTKA, Ref. No. K83133). S. Shelyag is grateful to ATST-EAST workshop organisers for providing help and financial support to attend the meeting. S. Shelyag is also grateful to R. Stein and M. Carlsson for helpful discussions during the meeting.

References

- Bonet, J. A., Márquez, I., Sánchez Almeida, J., Cabello, I., & Domingo, V. 2008, *ApJ*, 687, L131
- Clyne, J., Mininni, P., Norton, A., & Rast, M. 2007, *New Journal of Physics*, 9, 301
- Erdélyi, R., & Fedun, V. 2007, *Science*, 318, 1572
- Fedun, V., Shelyag, S., Verth, G., Mathioudakis, M., & Erdélyi, R. 2011, *Annales Geophysicae*, 29, 1029
- Fedun, V., Shelyag, S., & Erdélyi, R. 2011, *ApJ*, 727, 17
- Fedun, V., Verth, G., Jess, D. B., & Erdélyi, R. 2011, *ApJ*, 740, L46
- Jess, D. B., Mathioudakis, M., Erdélyi, R., et al. 2009, *Science*, 323, 1582
- Moll, R., Cameron, R. H., & Schüssler, M. 2011, *A&A*, 533, A126
- Rempel, M., Schüssler, M., Cameron, R. H., & Knölker, M. 2009, *Science*, 325, 171

- Shelyag, S., Schüssler, M., Solanki, S. K., Berdyugina, S. V., Vögler, A. 2004, *A&A*, 427, 335
- Shelyag, S., Schüssler, M., Solanki, S. K., Vögler, A. 2007, *A&A*, 469, 731
- Shelyag, S., Fedun, V., & Erdélyi, R. 2008, *A&A*, 486, 655
- Shelyag, S., Keys, P., Mathioudakis, M., & Keenan, F. P. 2011, *A&A*, 526, A5
- Shelyag, S., Fedun, V., Keenan, F. P., Erdélyi, R., & Mathioudakis, M. 2011, *Annales Geophysicae*, 29, 883
- Steiner, O., Rezaei, R., Schaffenberger, W., & Wedemeyer-Böhm, S. 2008, *ApJ*, 680, L85
- Vargas Domínguez, S., Palacios, J., Balmaceda, L., Cabello, I., & Domingo, V. 2011, *MNRAS*, 416, 148
- Vögler, A., Shelyag, S., Schüssler, M., Cattaneo, F., Emonet, T., & Linde, T. 2005, *A&A*, 429, 335
- Wedemeyer-Böhm, S., & Rouppe van der Voort, L. 2009, *A&A*, 507, L9
- Zaqarashvili, T. V., Khodachenko, M. L., & Rucker, H. O. 2011, *A&A*, 534, A93